Data Driven Evaluation of Inertial Support Distribution in a Heterogeneous Power System

Jasdeep Kour
Dept. of Electrical Engineering
Indian Institute of Technology Jammu
Jammu, India
jasdeep.kour@iitjammu.ac.in

Anup Shukla
Dept. of Electrical Engineering
Indian Institute of Technology Jammu
Jammu, India
anup.shukla@iitjammu.ac.in

***Abstract*—Accurate evaluation of inertial response is essential for the secure operation of renewable-rich power systems characterized by reduced and time-varying inertia. This paper proposes a practical, model-free, data-driven framework to quantify the spatiotemporal distribution of bus-level inertial support from synchronous generators, inverter-based resources, and dynamic loads. Three learning architectures—Bi-LRCNN, GCNN, and STGCNN—are developed to capture network-coupled spatial and temporal dependencies using time-synchronized PMU measurements. The framework is validated on modified IEEE test systems and further supported using field data from the Rajasthan renewable energy complex under diverse contingency scenarios. Optimal PMU placement ensures numerical observability, while physics-consistent supervisory labeling preserves physically realizable system dynamics. Comparative results demonstrate that STGCNN achieves the highest prediction accuracy of 98.45%, highlighting the effectiveness of spatiotemporal graph learning for real-time situational awareness in low-inertia grids.**

***Index Terms*—Bus inertia, graph convolution neural network, inertial response, inertial time frame, spatiotemporal**

I. Introduction

The increasing penetration of inverter-based resources (IBRs) has fundamentally transformed power-system dynamics by reducing physical inertia and introducing faster electromechanical transients. Low-inertia operating conditions increase the risk of frequency excursions, protection failure, and cascading failures, thereby necessitating continuous monitoring of the system's inertial response to support corrective actions, such as frequency containment reserves and synthetic inertia controls [1]-[2]. A broad spectrum of inertia-estimation methods has been reported in the literature. Conventional approaches primarily rely on disturbance-based analysis and swing-equation formulations using frequency and active-power measurements. While these methods typically assume known perturbations and accurate network parameters, they are limited in applicability to heterogeneous grids with high renewable penetration [3]–[7]. Recent studies extend inertia assessment to include contributions from inverter-based resources and demand-side dynamics; however, many focus on aggregated system behavior and fail to capture the spatial variability of inertial support across the network.

With the rapid expansion of phasor measurement unit (PMU) deployment, data-driven techniques have emerged as promising tools for real-time inertia estimation [8]–[13]. Existing learning-based approaches predominantly estimate total system inertia and often overlook bus-level dynamics within the inertial time frame. Furthermore, biased measurement placement and limited observability can restrict their practical deployment. Although some formulations treat bus inertia as synchronous generators do, they often neglect inertial contributions from loads and emulated sources, which are increasingly significant in renewable-rich systems [14]-[15]. Graph-based learning methods offer a powerful framework for modeling the non-euclidean structure of power networks by explicitly incorporating electrical connectivity. Variants of graph neural networks have demonstrated strong performance in applications such as power system prediction, renewable energy forecasting, and fault analysis [16]–[22]. However, existing studies have not adequately addressed evaluating bus-level inertial response within the inertial time frame using spatiotemporal graph architectures.

Although analytical formulations can estimate inertia when network parameters are precisely known, practical renewable-rich power systems increasingly operate under uncertain topology, dynamic inverter controls, measurement noise, and partially observable conditions. These factors limit the reliability of algebraic or least-squares-based approaches for real-time inertia evaluation. To address these challenges, a model-free, fully data-driven framework is developed that learns the nonlinear mapping between measurable system dynamics and bus-level inertial response directly from time-synchronized measurements while preserving physics consistency through supervisory labeling. Motivated by these gaps, the primary contributions of this work are summarized as follows:

1) A model-free, data-driven framework is proposed to quantify the spatiotemporal distribution of inertial support at each bus, capturing contributions from synchronous generators, inverter-based resources, and geographically distributed loads.
2) Spatiotemporal learning architectures are developed and validated using real-time datasets representing diverse grid conditions, including varying renewable penetration levels, contingency scenarios, and weak-grid operation.
3) Both grid-following and grid-forming modes of IBR operation are incorporated to ensure a realistic representation of converter behavior in modern power systems.

979-8-3315-8138-1

The remainder of this paper is organized as follows. Section II reviews the foundations of inertia estimation and learning. Section III presents the proposed methodology. Section IV discusses the results, and Section V concludes the paper.

II. Inertia Estimation and Learning Algorithms

In synchronous generator (SG)-dominated systems, inertia represents stored kinetic energy, whereas in the IBR-rich grids, it is emulated through control mechanisms. For a system comprising multiple SGs and loads, the augmented admittance matrix [15] is expressed as

$$\begin{bmatrix} \bar{i}_g(t) \\ \bar{i}_b(t) \end{bmatrix} = \begin{bmatrix} \bar{Y}_{gg} & \bar{Y}_{gb} \\ \bar{Y}_{bg} & \bar{Y}_{bb} \end{bmatrix} \begin{bmatrix} \bar{V}_g(t) \\ \bar{V}_b(t) \end{bmatrix}. \tag{1}$$

where $V_b(t)$, $i_b(t)$, $V_g(t)$, and $i_g(t)$ denote the bus and generator voltages and currents, respectively. Replacing the generator terminal voltage with its internal electromotive force (emf) behind internal impedance yields

$$\bar{V}_g(t) = \bar{e}_g(t) - \bar{i}_g \bar{Z}_g. \tag{2}$$

Substituting (2) into (1) and following the procedure in [21] gives

$$\begin{bmatrix} \bar{i}_g(t) \\ \bar{i}_b(t) \end{bmatrix} = [A] \begin{bmatrix} \bar{e}_g - \bar{i}_g \bar{Z}_g \\ \bar{V}_b(t) \end{bmatrix}. \tag{3}$$

Following [21], the load-bus frequency deviation is expressed as

$$\Delta\omega_b(t) = \Delta\omega_{wb}(t)\, \Delta\omega_g(t), \tag{4}$$

where $\Delta\omega_b(t)$, $\Delta\omega_{wb}(t)$, and $\Delta\omega_g(t)$ denote the load-bus frequency deviation vector, the weighted bus matrix, and the generator speed deviation vector, respectively. The weighted bus matrix represents the electrical coupling strength between generators and load buses and is derived from the reduced network admittance matrix. Each entry quantifies the relative influence of generator speed deviations on the corresponding bus frequency, thereby enabling the mapping of generator dynamics to bus-level inertial response. Similarly, the relationship between generator inertia and bus inertia is given by [15]

$$H_b(t) = \Delta\omega_c\, H_g(t), \tag{5}$$

where $H_b(t)$, $\Delta\omega_c$, and $H_g(t)$ denote the bus inertia, connection matrix, and generator-inertia matrix, respectively. The formulation in (5) accounts only for synchronous-generator inertia and neglects inertial support from loads and IBRs. Because representing these heterogeneous contributions through a single inertia constant is inadequate [14], evaluating post-contingency inertial response requires a framework capable of capturing nonlinear and network-coupled dynamics.

To address this limitation, three learning-based architectures—Bidirectional long recurrent convolution neural network (Bi-LRCNN), graph convolution neural network (GCNN), and spatiotemporal graph convolution neural network (STGCNN)—are developed, as illustrated in Fig. 1. These models are designed to learn the mapping between measurable system dynamics and bus-level inertial response while preserving the underlying network structure. The Bi-LRCNN combines convolutional neural networks (CNNs) for spatial feature extraction with bidirectional long short-term memory (Bi-LSTM) units to capture temporal dependencies [22]. Dropout regularization is incorporated to mitigate overfitting. Graph convolutional neural networks extend convolutional operations to non-euclidean domains, enabling explicit modeling of power system topology. Using an undirected heterogeneous graph representation, the graph convolution layer extracts structural dependencies and is expressed as

$$f(X, A) = \sigma(D^{-1/2}(A + I)D^{-1/2}XW), \tag{6}$$

where A, I, and D denote the adjacency, identity, and degree matrices, respectively. X represents the node feature matrix, W contains learnable weights, and $\sigma(\cdot)$ is the activation function.

The STGCNN further embeds temporal evolution by incorporating time-varying node features into the graph structure, enabling simultaneous learning of spatial and temporal correlations. While (6) captures spatial dynamics, the temporal update is defined as

$$H^{(t+1)} = \sigma(W_t H^t + b_t), \tag{7}$$

where H^t, W_t, and b_t denote the hidden state, learnable weight matrix, and bias at time t, respectively. As node features evolve over time, the corresponding graphs are updated, allowing STGCNN to identify latent spatiotemporal patterns and deliver improved prediction accuracy.

III. Proposed Methodology

Fig. 1 illustrates the overall workflow of the proposed framework. Time-synchronized measurements from optimally placed PMUs are used to construct node feature vectors that represent the dynamic state of each bus. These features are embedded into graph structures that preserve the network's electrical topology and are subsequently processed using Bi-LRCNN, GCNN, and STGCNN architectures to learn hidden spatial and temporal dependencies. The trained models estimate bus-level inertial support while disaggregating the contributions from SGs, inverter-based resources, and dynamic loads.

A. Input Feature Construction for Learning Models

The learning models utilize PMU measurements captured during the inertial time frame immediately following a disturbance. For each monitored bus, the node feature vector is defined as $X_b(t)$ where

$$X_b(t) = \left[V_b(t), \theta_b(t), f_b(t), \frac{df_b(t)}{dt}, P_b(t), Q_b(t) \right] \tag{8}$$

where $V_b(t)$ and $\theta_b(t)$ denote the voltage magnitude and phase angle, $f_b(t)$ represents the bus frequency, $\frac{df_b(t)}{dt}$ is the rate of change of frequency (ROCOF), and $P_b(t)$ and $Q_b(t)$ correspond to the active and reactive power injections at a bus, respectively. These features capture early frequency acceleration and electromechanical power imbalance following a contingency, which predominantly governs inertial response. Time-stacked feature sequences enable the models to learn transient dynamics while preserving spatial correlations imposed by network

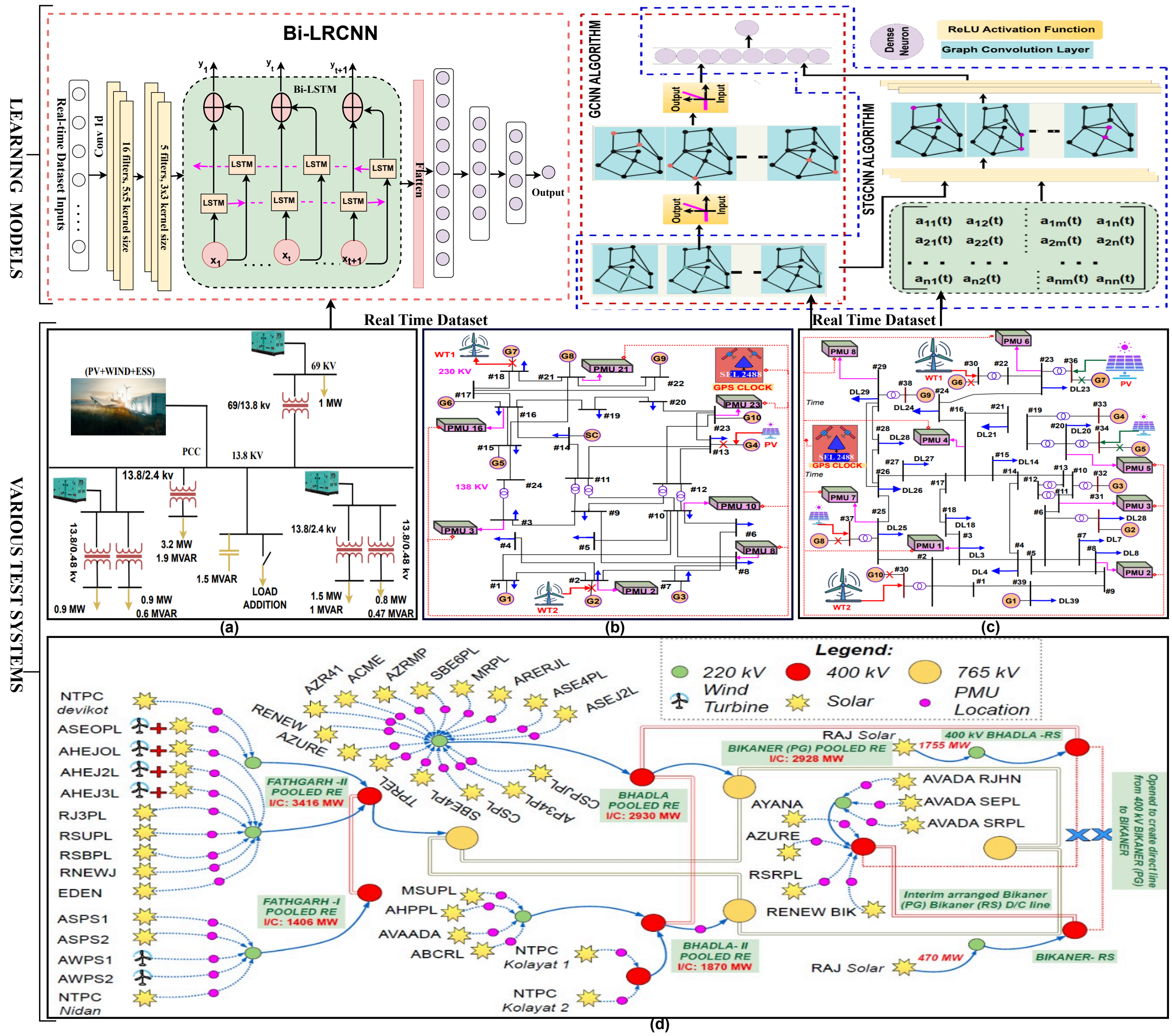

Fig. 1. Proposed system setup

connectivity. Prior to training, all features are normalized to improve numerical stability and convergence. The proposed method estimates post-disturbance inertial support at each bus and separates the contributions from SGs, IBRs, and loads as

$$\Delta P_b(t) = W_1 \Delta P_{b_{SG}}(t) + W_2 \Delta P_{b_{NSG}}(t) + W_3 \Delta P_{b_L}(t) \quad (9)$$

where W_1, W_2, and W_3 denote the respective connection matrices. PMUs are optimally placed to ensure numerical observability [23]. The cumulative SG response at any bus is expressed as

$$\Delta P_{SG}(t) = \sum_{i=1}^{m} \Delta P_i(t), \qquad \Delta P_{b_{SG}}(t) = W_1 \Delta P_{SG}(t) \quad (10)$$

The inertial load support includes contributions from frequency- and voltage-dependent loads:

$$\Delta P_f(t) = k\, P_L(t) \Delta f(t), \qquad \Delta P_v(t) = P_v(t) - \sum_{i=1}^{l} P_i, \quad (11)$$

$$\Delta P_L(t) = \Delta P_f(t) + \Delta P_v(t), \quad (12)$$

with the corresponding bus-level contribution given by

$$\Delta P_{b_L}(t) = W_3 \Delta P_L(t). \quad (13)$$

The inertial support from non-synchronous resources is obtained by rearranging (9):

$$W_2 \Delta P_{b_{NSG}}(t) = \Delta P_b(t) - (W_1 \Delta P_{b_{SG}}(t) + W_3 \Delta P_{b_L}(t)) \quad (14)$$

979-8-3315-8138-1

TABLE I
CUMULATIVE INERTIAL CONTRIBUTIONS DURING THE INERTIAL TIME FRAME

IBR Integrated	IBR Pen. (%)	Contingency	Load IR(MW)	IBR IR(MW)
1 PV (G5)	0–10	SG (G8) Trip Load (DL7) Trip	187.5 96.26	87.12 44.37
1 PV (G5) + 1 WT (G6)	10–20	SG (G8) Trip Load (DL23) Trip	222 123.25	163 94
PV at G5 & G8	10–20	SG (G7) Trip Load (DL23) Trip	210.11 112.5	159.62 75.32
WT at G6 & G10	10–20	SG (G8) Trip Load (DL23) Trip	200 85.41	135 67.11
2 WT + 1 PV	>20	SG (G7) Trip Load (DL7) Trip NSG (PV G5) Trip	368.25 184.5 217.32	240 122.62 178

Supervisory labels used for training are derived from the post-contingency power imbalance relationships defined in (9)–(13). This physics-consistent labeling ensures that the learning process remains anchored to realizable system dynamics while enabling the models to approximate nonlinear mappings that are difficult to capture analytically.

IV. RESULTS AND VALIDATION

The proposed framework is validated on multiple benchmark systems and field datasets to assess its effectiveness in estimating bus-level inertial response under diverse operating conditions. Although the STGCNN architecture achieves the highest prediction accuracy, it requires greater training effort due to graph convolution and temporal feature propagation. Training is performed offline, whereas inference requires only milliseconds, making the framework suitable for real-time situational awareness. Simpler architectures, such as ANN and CNN, impose a lower computational burden but fail to capture network-coupled dynamics adequately, thereby justifying the use of spatiotemporal graph learning.

A. Estimation of Cumulative Inertial and IBR Response During the Inertial Time Frame

Table I summarizes the cumulative inertial contributions from SGs, IBRs, and loads for the MI-39BS across varying renewable penetration levels. At low penetration (0–10%), SGs supply most of the imbalance, whereas beyond 20% penetration, the response becomes increasingly dominated by fast-emulated support from IBRs. This transition highlights the evolving dynamics of renewable-rich grids. Unlike prior work that considers partial observability, the present study adopts optimal PMU placement to ensure numerical observability and improve estimation reliability. The impact of inertial control is also examined by operating PV and wind turbine units in reserve mode (R_{Mode}) [24], enabling enhanced post-contingency support.

B. Computation of Bus Inertial Response

Table II reports the predicted inertial support at individual buses. Across datasets representing diverse system configurations, STGCNN consistently achieves the lowest mean squared error, confirming its superior ability to learn coupled spatiotemporal dependencies. IBRs are integrated using both grid-following (GFL) and droop-based grid-forming (GFM) strategies [24]. Weak-grid conditions are emulated by increasing renewable penetration beyond 30%, thereby exposing the models to enriched dynamic scenarios. Hyperparameter tuning ensures robust performance across operating conditions.

While optimal PMU placement guarantees numerical observability, additional analysis indicates that prediction accuracy degrades gracefully under moderate reductions in measurement density, suggesting practical applicability even when ideal PMU coverage is unavailable.

C. Validation Using the Rajasthan Renewable Energy Complex

The framework is further validated using field measurements from the Rajasthan renewable energy complex, which comprises large-scale solar and hybrid installations interconnected via multi-voltage transmission corridors [1]. Contingency datasets provided by Grid Controller of India Limited were used for training and evaluation. Results in Table III demonstrate strong agreement between predicted and measured inertial support across disturbance events, confirming the practical applicability of the proposed approach for real-world renewable-rich grids. The mean squared error (MSE) is used as the evaluation metric [25].

V. CONCLUSION

This paper proposes a data-driven, model-free framework to estimate the geo-temporal inertial response of power systems by capturing contributions from SGs, IBRs, and dynamic loads. Learning models are trained on real-time datasets that reflect varying renewable penetration levels, contingencies, and operating states. Among the models, STGCNN achieves the highest accuracy in estimating bus-level and system-wide inertial responses, as validated using field data from the Rajasthan renewable energy complex. The results are consistent with expected converter behavior in both grid-following and forming modes, demonstrating the practicality of data-driven approaches for stability assessment in low-inertia grids. The proposed method offers a scalable real-time solution for improved situational awareness and adaptive grid operation in renewable-rich systems.

REFERENCES

[1] Report on Events Involving Transmission Grid Connected Wind and Solar Power Plants, Grid Controller of India Limited, Nov. 2023.

[2] D. Wilson, J. Yu, N. Al-Ashwal, B. Heimisson, and V. Terzija, “Measuring effective area inertia to determine fast-acting frequency response requirements,” *Int. Journal of Electrical Power Energy Syst.*, vol. 113, pp. 1-8, 2019.

[3] P. Wall and V. Terzija, “Simultaneous estimation of the time of the disturbance and inertia in power systems,” *IEEE Trans. Power Del.*, vol. 29, no. 4, pp. 2018-2031, Aug. 2014.

[4] P. M. Ashton, C. S. Saunders, G. A. Taylor, A. M. Carter, and M. E. Bradley, “Inertia estimation of the GB power system using synchrophasor measurements,” *IEEE Trans. Power Syst.*, vol. 30, no. 2, pp. 701-709, Mar. 2015.

[5] J.Zhang and H. Xu, “Online Identification of Power System equivalent inertia constant,”*IEEE Trans. on Industrial Elec.*,vol 64, no. 10 pp. 8098 - 8107, 2017.

[6] J. Kour and A. Shukla, “Inertia estimation techniques in a solar PV integrated distribution system,” 2023 IEEE IAS Global Conference on Renewable Energy and Hydrogen Technologies (GlobConHT), Male, Maldives, pp. 1-6, Mar. 2023.

979-8-3315-8138-1

TABLE II
EVALUATION OF INERTIAL SUPPORT AT A BUS DURING INERTIAL TIME FRAME USING VARIOUS MODELS

System	Bus	IBR Penetration % and Type	Contingency Condition	Evaluation Model	Actual Bus Inertial Support (MW)	Predicted Bus Inertial Support(MW)	MSE%	System Stability
MI-DS	At PCC	$>$ 10 % and GFL	DG1 Trip	ANN	0.23256949	0.23673558	5.96	Stable
				CNN		0.22749451	9.16	
				RNN		0.14317246	7.86	
				Bi-LRCNN		0.23153824	0.44	
				GCNN		0.23712588	0.11	
				STGNN		0.23664525	0.09	
MI-24BS	BUS 16 - 19	(10 - 20) % and GFL	G8 Tripping	ANN	0.22515042	0.25516432	12.33	Stable
				CNN		0.22615683	1.24	
				RNN		0.26214458	2.42	
				Bi-LRCNN		0.21987823	1.41	
				GCNN		0.22772282	0.71	
				STGNN		0.22549139	0.151	
MI-24BS	BUS 18- 21	(10 - 20) % droop based GFM	G8 Tripping	ANN	0.63009068	0.62128866	2.83	Stable
				CNN		0.61978995	2.45	
				RNN		0.61984598	2.44	
				Bi-LRCNN		0.62996107	1.24	
				GCNN		0.62919186	0.5	
				STGNN		0.63000000	0.1	
MI-39BS	BUS 16 - 19	(0 - 10) % and GFL	G8 Tripping	ANN	0.14809747	0.16291138	18.56	Stable
				CNN		0.15809628	12	
				RNN		0.15317246	7.86	
				Bi-LRCNN		0.15196016	2.608	
				GCNN		0.14992112	0.34	
				STGNN		0.14805000	0.11	
MI-39BS	BUS 22 - 23	(0 - 10) % and droop based GFM	G8 Tripping	ANN	0.12918312	0.13542321	9	Stable
				CNN		0.13211218	4.53	
				RNN		0.13242322	5.01	
				Bi-LRCNN		0.1300870	1.44	
				GCNN		0.12892311	0.201	
				STGNN		0.12907522	0.167	
MI-39BS	BUS 18 - 3	$>$ 30 % and GFL	DL 20 Tripping	ANN	0.14881917	0.15623112	9.96	Stable yet weak grid
				CNN		0.15496016	8.25	
				RNN		0.13317246	10.02	
				Bi-LRCNN		0.14921672	0.46	
				GCNN		0.14921672	0.26	
				STGNN		0.14891612	0.18	

TABLE III
EVALUATION OF INERTIAL SUPPORT AT A BUS DURING INERTIAL TIME FRAME USING VARIOUS MODELS FOR RAJASTHAN RE COMPLEX

Bus	Date of Event	Contingency Condition	Evaluation Model	Actual Bus Inertial Support (MW)	Predicted Bus Inertial Support (MW)	MSE%
Bhadla2-Ajmer	9 thFeb 2023	R-Y fault	Bi-LRCNN	0.458	0.38	5.02
			GCNN		0.423	1.89
			STGNN		0.448	0.29
Bhadla - Bikaner	9 th Feb 2023	Line Reactor Opening	Bi-LRCNN	0.128	0.176	0.47
			GCNN		0.189	0.12
			STGNN		0.126	0.05
Bhadla-Azure Mapple ckt	15 th May 2023	Y-B fault	Bi-LRCNN	0.562	0.516	1.52
			GCNN		0.535	0.628
			STGNN		0.559	0.12

[7] Y. Bian, H. Wyman-Pain, F. Li, R. Bhakar, S. Mishra and N. P. Padhy, "Demand side contributions for system inertia in the GB power system,"*IEEE Trans. Power Syst.*, vol. 33, no. 4, pp. 3521-30, Jul. 2018.

[8] J. Guo, X. Wang, and B.-T. Ooi, "Estimation of inertia for synchronous and non-synchronous generators based on ambient measurements," *IEEE Trans. Power Syst.*, vol. 37, no. 5, pp. 3747-3757, Sep. 2022.

[9] T. Kerdphol, M. Watanabe, R. Nishikawa, Y. Hayashi, Y. Mitani, "Inertia estimation of the 60 Hz Japanese power system from synchrophasor measurements," *IEEE Trans. Power Syst.*, vol. 38, no. 1, pp. 753 - 766, Jan. 2023.

[10] D.Yang, B. Wang, G. Cai, Z. Chen, J. Ma, Z. Sun, L. Wang, "Data-driven estimation of inertia for multiarea interconnected power systems using dynamic mode decomposition," *IEEE Trans. Ind. Inform.*, vol. 17, no. 4, pp. 2686 - 2695, April 2021.

[11] Alvaro J. Hernandez M, R.T. Pinto, "Artificial neural network- based inertia estimation," *IEEE Power & Energy Society General Meeting*, pp. 1-5, July 2022.

[12] M. Tuo, X. Li, "Machine learning assisted inertia estimation using ambient measurements," *IEEE Trans. Industry App.*, vol. 59, no. 4, pp. 4893 - 4903, July-Aug 2023.

[13] M. Mazidi, T. McKelvey, P. Chen, "A pure data-driven method for online inertia estimation in power systems using local rational model approach," *IEEE Trans. Industry App.*, vol. 59, no. 5, pp. 5506 - 5516, Sept-Oct 2023.

[14] P.K. Dhara, Z.H. Rather, "Non-synchronous inertia estimation in a renewable energy integrated power system with reduced number of monitoring nodes," *IEEE Trans. Sust. Energy*, vol. 14, no. 12, pp. 864 - 875, April 2023.

[15] S. Ghosh, Y. J. Isbeih, M. S. El Moursi, "Assessment of bus inertia to enhance dynamic flexibility of hybrid power systems with renewable energy integration," *IEEE Trans. Power Del.*, vol. 38, Issue 4, pp. 2372 - 2386, Aug 2023.

[16] Z. Wu, S. Pan, F. Chen et al., "A comprehensive survey on graph neural networks," *IEEE Trans. on Neural Networks and Learning Syst.*, vol. 32, no. 1, pp. 4-24, Jan. 2021.

[17] Z. Yingran, L. Chao and S. Rui, "Enhancing Traffic Flow Forecasting With Delay Propagation: Adaptive Graph Convolution Networks for Spatio-Temporal Data," *IEEE Trans. on Intelligent Transportation Syst.*, vol. 26, no. 1, pp. 650-660, Jan. 2025

[18] M. Khodayar, G. Liu, J. Wang et al., "Deep learning in power systems research: a review," *CSEE Journal of Power and Energy Syst.*,Vol. 7, No. 2, March 2021.

[19] C. Qin, A. K. Srivastava, A. Y. Saber, D. Matthews and K. Davies, "Geometric Deep-Learning-Based Spatiotemporal Forecasting for Inverter-Based Solar Power," *IEEE Syst. Journal*, vol. 17, no. 3, pp. 3425-3435, Sept. 2023.

[20] A. Dwivedi and A. Tajer, "GRNN-Based Real-Time Fault Chain Prediction," *IEEE Trans. Power Syst.*, vol. 39, no. 1, pp. 934-946, Jan. 2024.

[21] X. Jin et al., "Graph Spatio-Temporal Networks for Condition Monitoring of Wind Turbine," *IEEE Trans. Sust. Energy*, vol. 15, no. 4, pp. 2276-2286, Oct. 2024

[22] M.Ma and Z.Mao, "Deep-convolution-based LSTM network for remaining useful life prediction," *IEEE Trans. Ind. Inform.*, vol.17, no. 3, pp. 1658-1667, May 2020.

[23] G. N. Korres, P. J. Katsikas, K. A. Clements,P. W. Davis, "Numerical observability analysis based on network graph theory," *IEEE Trans. Power Syst.*, vol. 18, No. 3, pp. 1035-1045, Aug 2003.

[24] B. Pawar, E. I. Batzelis, S. Chakrabarti, B.C. Pal, "Grid-forming control for solar PV systems with power reserves," *IEEE Trans. Sust. Energy*, vol. 12, Issue 4, pp. 1947-1959, Oct. 2021.

[25] A. Chugh, "MAE, MSE, RMSE, coefficient of determination, adjusted R-squared—which metric is better" Dec 8, 2022.